The Cosmic Microwave Background Spectrum – an Analysis

H. P. Nordberg[1]

Abstract

This work presents a detailed analysis of the Cosmic Microwave Background (CMB) radiation intensity observations. The CMB is a relic of the Big Bang and the study of it greatly enhances our knowledge of our universe of today and of yesterday. This work has led to new limits on parameters such as the temperature of the CMB, the speed of our solar system relative to the CMB and a few other cosmologically important parameters. Detailed observations and analysis of the CMB spectrum provide tight constraints on the thermal history of the universe and the release of energy in early epochs.

1 Introduction

1.1 The Cosmic Microwave Background Radiation

Early nucleosynthesis[2] calculations by Gamow, Alpher and Herman [Alpher & Herman 1988] showed that, from the theory of a hot big bang, one can infer a cosmic microwave background radiation (CMB) to be present today as a result of the primordial fireball. The spectrum was predicted to be of black body form with a temperature of a few Kelvin. In 1964, Penzias and Wilson [Penzias & Wilson 1965] discovered this radiation, measuring a "background noise" of 3K. They were then not aware of the theory but, as luck would have it, radio astronomer Bernie Burke suggested they contact Dicke's Princeton team, which

[1]Lund University, Dept. of Physics, Sölvegatan 14, Lund, Sweden & LBNL, Bldg 50-351, University of California, Berkeley CA 94720, HNordberg@lbl.gov

[2]See Appendix A for a definition of nucleosynthesis and entities that are used through out the text.

currently was working on detecting the CMB. They did, and published companion papers in 1965 in Astrophysical Journal [Dicke *et al.* 1965, Penzias & Wilson 1965].

Thermodynamic equilibrium was reached early after the Big Bang as a result of very rapid interaction during the inflationary era. The shape of the Planck distribution, Fig. 1, is invariant under the universal expansion since interaction is rapid enough to create and maintain the Planck distribution in the very early universe. After decoupling, the photon number is conserved, so the occupation number, $n = 1/\left(\exp\left(\frac{h\nu}{kT}\right) - 1\right)$, and therefore $\frac{h\nu}{kT}$ are constant. Redshift, z, is defined as fractional change in wavelength $z \equiv (\lambda' - \lambda)/\lambda$, due to the Doppler effect, so $\nu'/\nu = \lambda'/\lambda = 1 + z$. Thus, a Planck distribution of temperature T_i at redshift z_i transforms into another Planck distribution of temperature T_f at redshift z_f. T_i and T_f are then related by

$$\frac{T_\mathrm{i}}{1 + z_\mathrm{i}} = \frac{T_\mathrm{f}}{1 + z_\mathrm{f}}.$$

Therefore we expect the CMB spectrum to be Planckian today and, indeed, to a large extent it is.

The CMB spectrum would have a blackbody form if the simple, hot Big Bang model is a correct description of the early universe, but could be distorted from that form by energy release for a redshift $z \lesssim 3 \times 10^6$ [Sunyaev & Zeldovich 1980, Smoot *et al.* 1988]. Such releases might arise from decay of unstable particles, dissipation of cosmic turbulence and gravitational waves, breakdown of cosmic strings and other more exotic transformations. The CMB was the dominant energy field after the annihilation of positrons and the decoupling of neutrinos until $z \gtrsim 3 \times 10^4$ [Fixsen *et al.* 1996]. For energy release, into the electron-proton plasma, between redshift of a few times 10^4 and 10^6 [Smoot *et al.* 1988] the number of Compton scatterings is sufficient to bring the photons into thermodynamic equilibrium with the primordial plasma. During this time, Bremsstrahlung and other radiative processes do not have enough time to create a sufficient number of photons to make a Planck distribution.

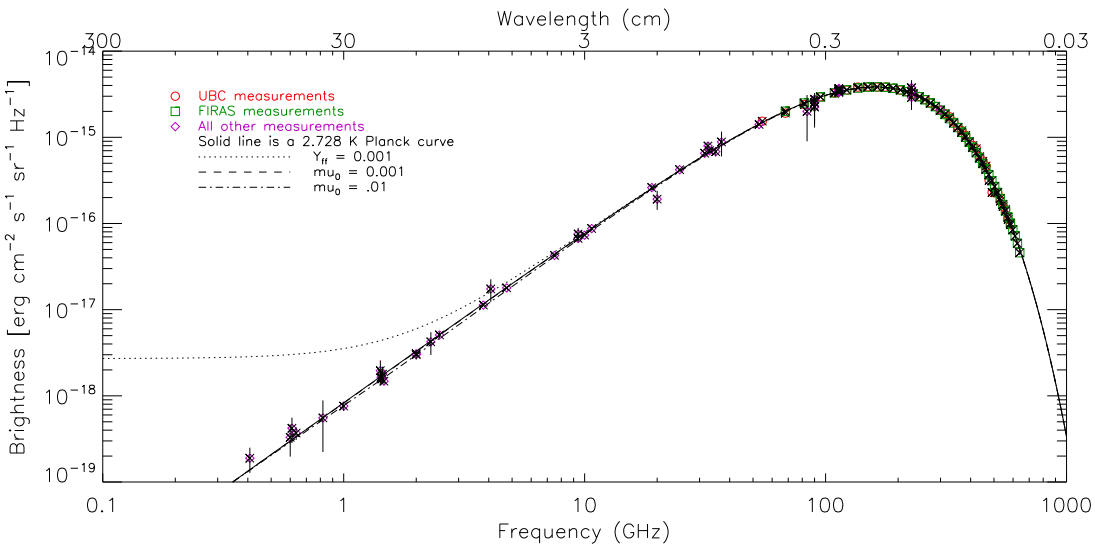

Figure 1: Brightness as a function of frequency of the CMB, including all measurements up till now.

The resulting distribution is a Bose-Einstein spectrum with a chemical potential, μ, that is exponentially attenuated at low frequencies, $\mu = \mu_0 e^{-2\nu_b/\nu}$ (where ν_b is the frequency at which Compton scattering of photons to higher frequencies is balanced by Bremsstrahlung creation at lower frequencies [Danese & De Zotti 1982]). At redshifts smaller than a few times 10^4, the Compton scattering rate is no longer sufficiently high to produce thermodynamic equilibrium and a Bose-Einstein spectrum. The resulting spectrum has an increased brightness temperature in the far Rayleigh-Jeans region due to Bremsstrahlung emission by relatively hot electrons, a reduced temperature in the middle Rayleigh-Jeans region where the photons are depleted by Compton scattering, and a high temperature in the Wien region where the Compton-scattered photons have accumulated.

Table 1: Nonlinear fit of T_0, $Y_{\rm ff}$, μ_0, y and β. $\chi^2 = 259$ with 201 degrees of freedom.

T_0	=	2.7356	$\pm$ 0.0037 K	(95% CL)
$Y_{\rm ff}$	=	-1.1×10^{-5}	$\pm$ 2.3×10^{-5}	(95% CL)
μ_0	=	-3.1×10^{-5}	$\pm$ 1.2×10^{-4}	(95% CL)
y	=	1.6×10^{-6}	$\pm$ 9.6×10^{-6}	(95% CL)
β	=	1.2293×10^{-3}	$\pm$ 4.9×10^{-6}	(95% CL)

$$\text{Correlation matrix} = \begin{array}{c} \\ T_0 \\ Y_{\rm ff} \\ \mu_0 \\ y \\ \beta \end{array} \begin{array}{c} \begin{array}{ccccc} T_0 & Y_{\rm ff} & \mu_0 & y & \beta \end{array} \\ \left[\begin{array}{ccccc} 1.00 & 0.01 & 0.05 & 0.09 & 0.27 \\ 0.01 & 1.00 & -0.27 & -0.18 & 0.01 \\ 0.05 & -0.27 & 1.00 & 0.82 & -0.01 \\ 0.09 & -0.18 & 0.82 & 1.00 & 0.00 \\ 0.27 & 0.01 & -0.01 & 0.00 & 1.00 \end{array}\right] \end{array}$$

1.2 Current Results

The results of this work are new limits on the cosmological parameters

T_0 – the thermodynamic temperature of the background radiation

β – the quotient of the speed of our solar system to the speed of light, c

$Y_{\rm ff}$ – a measure of the effects of Bremsstrahlung, unitless; a.k.a. $J_{\rm ff}$

y – a measure of the effects of Compton scattering, unitless

μ_0 – describes the Bose-Einstein distortion, unitless.

The latter three parameters are explained in section 2.1, The Distortions. This thesis describes how these parameters are determined from the knowledge of the brightness of the CMB and the dipole. The dipole appears because the earth moves relative to the CMB.

The most complete fit is a nonlinear simultaneous fit of T_0, $Y_{\rm ff}$, μ_0, y and β, as shown

Table 2: Linear fit with T_0, $Y_{\rm ff}$, μ_0 and y

T_0	=	2.7356	$\pm$	0.0038 K	(95% CL)
$Y_{\rm ff}$	=	-1.1×10^{-6}	$\pm$	2.3×10^{-5}	(95% CL)
μ_0	=	-3.0×10^{-5}	$\pm$	1.2×10^{-4}	(95% CL)
y	=	1.6×10^{-6}	$\pm$	9.6×10^{-6}	(95% CL)

$$\text{Correlation matrix} = \begin{array}{c} \\ T_0 \\ Y_{\rm ff} \\ \mu_0 \\ y \end{array} \begin{array}{c} \begin{array}{cccc} T_0 & Y_{\rm ff} & \mu_0 & y \end{array} \\ \left[\begin{array}{cccc} 1.00 & 0.03 & -0.02 & 0.00 \\ 0.03 & 1.00 & -0.28 & -0.18 \\ -0.02 & -0.28 & 1.00 & 0.82 \\ 0.00 & -0.18 & 0.82 & 1.00 \end{array}\right] \end{array}$$

in Table 1, making use of all data published for the CMB monopole and dipole. The data are dominated by the COBE FIRAS [Fixsen *et al.* 1996] and the COBE DMR [Lineweaver *et al.* 1996] measurements for the monopole and the dipole respectively.

Table 2 contains the best-fitted values of T_0, $Y_{\rm ff}$ and μ_0. That fitting was done using both monopole and dipole data with linearized theory (see section 4.2 below). Table 1 includes y and β, as well as the parameters in Table 2. All measurements of the CMB monopole are plotted in Figure 1 – background flux versus frequency, Figure 2 – temperature versus frequency and Figure 7 – a close-up of the most interesting part of Figure 2. The dipole is plotted in Figure 3 – dipole temperature versus frequency, Figure 8 – a close-up of Figure 3 and Figure 6 – dipole antenna temperature versus frequency. See section 3 for more details on how the results were attained.

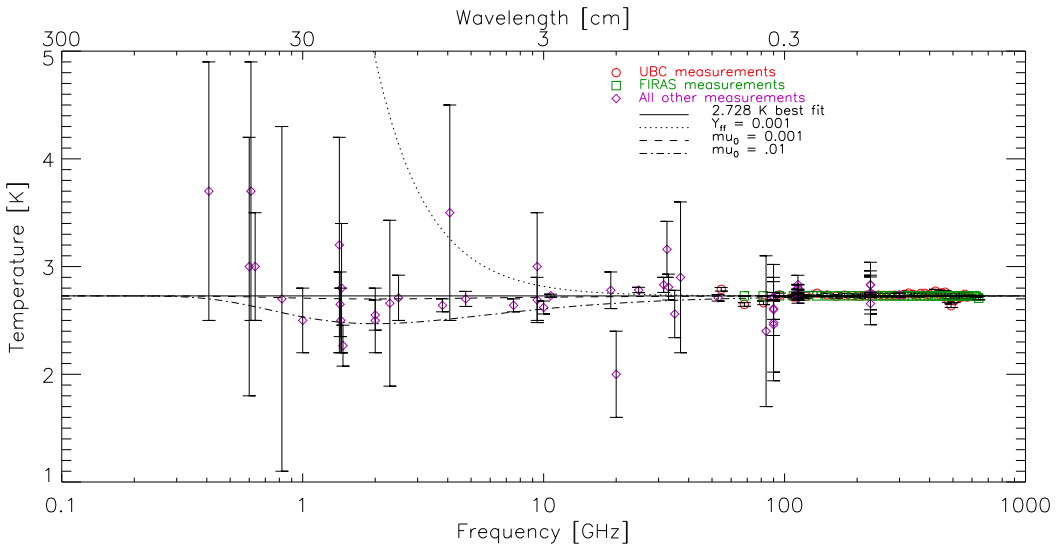

Figure 2: Thermodynamic temperature as a function of frequency for all CMB measurements up till now.

2 Theory

Since the thermodynamic temperature, T, unambiguisly specifies the Planckian distribution, $n = 1/\left(\exp\frac{h\nu}{kT} - 1\right)$, it is sometimes used when fitting to the different distortion parameters. In that respect, the thermodynamic temperature is equivalent to the brightness spectrum. In the following, the thermodynamic temperature is sometimes used to describe the distortions.

2.1 The Distortions

There are three important distortions, Compton (y), chemical potential (μ) and free-free (or Bremsstrahlung, $Y_{\rm ff}$).

Compton scattering ($\gamma e \rightarrow \gamma' e'$) of the background photons by a hot electron gas, creates spectral distortions by transferring energy from the electrons to the photons. The Compton distortion is characterized by the u parameter, here z is redshift and t time,

$$u = -\int_0^z \frac{kT_{\rm e}(z') - kT_\gamma(z')}{m_{\rm e}c^2}\sigma_{\rm T} n_{\rm e}(z') c \frac{dt}{dz'} dz' \tag{1}$$

where $\int_0^{t_0} \sigma_{\rm T} n_{\rm e}(z') c dt$ is the number of interactions and $(kT_{\rm e}(z') - kT_\gamma(z'))/m_{\rm e}c^2$ is the mean fractional photon-energy change per collision [Sunyaev & Zel'dovich 1980]. $\sigma_{\rm T}$ is the Thomson crossection, which is valid in the approximation that $h\nu \ll m_{\rm e}c$ in the rest frame of the electron. $n_{\rm e}$ is the electron number density. In the literature it is more common to use y

$$y = -\int_0^z \frac{kT_{\rm e}(z')}{m_{\rm e}c^2}\sigma_{\rm T} n_{\rm e}(z') c \frac{dt}{dz'} dz' \tag{2}$$

as a parameter rather than u. For $T_\gamma \ll T_{\rm e}$, $y \approx u$. For $ux^2 \ll 1$, where $x \equiv \frac{h\nu}{kT}$, Danese and DeZotti [Danese & DeZotti 1978] found that

$$n_{\rm Compton} \approx \frac{1}{e^x - 1}\left\{1 + u\frac{xe^x}{e^x - 1}\left[\frac{x}{\tanh x/2} - 4\right]\right\}. \tag{3}$$

Each Compton scattering changes the average fractional photon energy by an amount $\frac{kT_{\rm e}}{m_{\rm e}c^2}$ so when $\int_0^{t_0} \sigma_{\rm T} n_{\rm e}(z') c dt \cdot \frac{kT_{\rm e}}{m_{\rm e}c^2} > 1$, the photons and the electrons will have reached statistical equilibrium (as opposed to thermodynamic equilibrium) and the photon distribution is a Bose-Einstein distribution with a dimensionless chemical potential, μ

$$n_\mu = \frac{1}{e^{x+\mu} - 1} \tag{4}$$

where $x \equiv h\nu/kT$ is the dimensionless frequency. The chemical potential arises from the fact that the number of photons is conserved during Compton scattering, but the average energy per photon increases.

The equilibrium Bose-Einstein distribution results from the oldest non-equilibrium processes (a few times $10^4 < z < 8 \times 10^6$) [Smoot 1996], such as the decay of relic particles or primordial inhomogeneities.

Another effect of the hot electrons is Bremsstrahlung (or free-free radiation)

$$eZ \;\rightarrow\; e'Z'\gamma,$$

where Z denotes an ion. The electrons radiate as they are retarded or accelerated in collisions with themselves and other constituents of the primordial plasma, *e.g.*, protons. Free-free photons are created at low frequencies, and non-radiative Compton-scattering migrates their energy too slowly, so that they thermalize the spectrum to the electron temperature at low frequencies. Taking this effect into account, we have a frequency dependent chemical potential

$$\mu(x) = \mu_0 e^{-2x_{\rm b}/x} \tag{5}$$

where $x_{\rm b}$ is the frequency at which Compton scattering of photons to higher frequencies is balanced by free-free creation at low frequencies.

The free-free spectrum is described by the $Y_{\rm ff}$ parameter

$$n_{\rm Y_{ff}} = \frac{1}{e^{x/(1+Y_{\rm ff}/x^2)} - 1}. \tag{6}$$

2.2 The Dipole

Because the earth orbits the sun, the sun orbits in our galaxy and our galaxy moves relative to distant matter, we can have a net velocity with respect to the background radiation. The Doppler effect gives a *dipole anisotropy*, which, if we convert into thermodynamic temperature, measures 3.363 ± 0.0045 mK[3] (95% CL) in the direction (l, b)[4] $= (264.31^\circ \pm 0.04^\circ \pm 0.16^\circ, 48.05^\circ \pm 0.02^\circ \pm 0.09^\circ)$, where the first uncertainties are statistical and the second are systematical [Lineweaver *et al.* 1996]. It implies a speed of our solar system, again with respect to the background radiation, of 369 ± 1.5 km/s (95% CL). Adding

[3]Result from this work

[4]Galactic coordinates

this vector to that of the solar system with respect to the Local Group, $v_{\odot,\mathrm{LG}} = 316 \pm 10$ km/s $(l, b) = (93 \pm 4°, -4 \pm 4°)$ (95% CL) [AJ **111**, 794, 1996], we find that the Local Group of galaxies is heading, at a speed of 633.9 ± 10 km/s (95% CL), towards the Great Attractor located close to the Andromeda constellation, *i.e.* $(l, b) = (269° \pm 4°, 28° \pm 4°)$ (95% CL).

The Doppler and the relativistic effects change T so that observers with a velocity $\vec{\beta} \equiv \vec{v}/c$ through a Planckian radiation field of temperature T_0, will measure directionally dependent temperatures

$$T_{\mathrm{obs}}(\theta) = T_0 \frac{\sqrt{1-\beta^2}}{1-\beta\cos\theta}, \tag{7}$$

where θ is the angle between $\vec{\beta}$ and the direction of observation as measured in the observer's frame [Peebles 1993].

An observer in an isotropic photon distribution, $n(\nu)$, will measure a difference, Δn, between the intensity received in the direction of motion and that received in a direction perpendicular to its motion that follows [Forman 1970]

$$\Delta n = n \frac{d\ \ln n}{d\ \ln \nu} \beta. \tag{8}$$

Thus, we see that dipole anisotropy is frequency dependent and this gives us an opportunity to detect or set limits on distortion parameters such as μ, Y_{ff} and y.

To the first order in β, the dipole anisotropy of the CMB intensity is

$$\begin{aligned} T_d &= T_\nu - T_{\nu(1+\beta)} \\ &= \frac{h\nu}{k}\left[\ln^{-1}\left(1+\frac{1}{n(\nu)}\right) - \ln^{-1}\left(1+\frac{1}{n(\nu\,[1+\beta])}\right)\right] \\ &\approx -\frac{h\nu}{k(1+n)} \ln^{-2}\left(1+\frac{1}{n}\right) \frac{d\ \ln n}{d\ \ln \nu}\beta. \end{aligned} \tag{9}$$

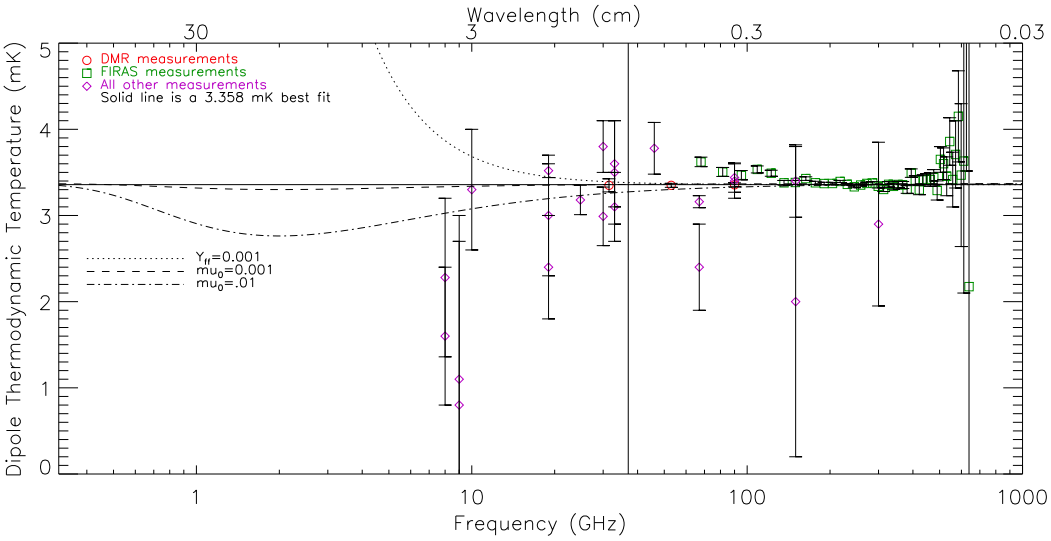

Figure 3: Thermodynamic temperature as a function of frequency of the CMB dipole.

For a Planck spectrum, $n = 1/(e^x - 1)$, this gives the dipole temperature as

$$T_d \approx T\beta \quad \left(\equiv T\frac{v}{c}\right). \tag{10}$$

Inserting the Bose-Einstein spectrum, eq. (4), into eq. (9), we get

$$T_{d,\mu} \approx T\beta \frac{x^2}{(x+\mu)^2}\left(1 + \mu\frac{2x_b}{x^2}\right). \tag{11}$$

Similarly, inserting the spectrum with the free-free distortion, eq. (6), into eq. (9) gives

$$T_{d,Y_{\rm ff}} \approx 3T\beta\frac{Y_{\rm ff}}{x^2}. \tag{12}$$

The Bose-Einstein and free-free distortions are plotted in fig. 3.

3 Method

The bulk of this work has been developing and deploying efficient regression routines in FORTRAN. This section discusses some of the methods used. What method is appropriate for a certain set of data varies from case to case, but a general discussion is nevertheless useful.

The matrix equations in the following text have been written as sums for easy conversion to computer codes. $\vec{v}$ denotes a vector and $\mathbf{M}$ a matrix.

3.1 The Basics of χ^2 Fitting

With x_i and y_i measured we assume that each y_i is drawn from a Gaussian distribution with mean $y_0(x_i)$ and standard deviation σ_i. As an example, our model may be $y_0(x) = a_0 + b_0 x$.

With the Gaussian assumption, the probability P_i for making the observed measurement y_i with standard deviation σ_i around the actual value $y_0(x_i)$ is

$$P_i = \frac{1}{\sigma_i\sqrt{2\pi}} e^{-\frac{1}{2}\left[\frac{y_i - y_0(x_i)}{\sigma_i}\right]^2}. \tag{13}$$

The probability for making the observed set of measurements of N values of y_i, when all σ_i's are independent, is the product of the probabilities for each individual observation

$$P(a_0, b_0) = \prod_i^N P_i = \prod_i^N \left\{ \left(\frac{1}{\sigma_i\sqrt{2\pi}} \right) e^{-\frac{1}{2}\left[\frac{y_i - y_0(x_i)}{\sigma_i}\right]^2} \right\}. \tag{14}$$

We assume that the observed set of measurements is more likely to have come from the distribution $y_0(x) = a_0 + b_0 x$ than from any other distribution with different coefficients, so $P(a_0, b_0)$ is the maximum probablility attainable with $P(a, b)$. Thus the *maximum-likelihood* for a and b are those that maximize $P(a, b)$.

Examining $P(a,b)$ we see that it suffices to minimize

$$\chi^2 \equiv \sum_i^N \left[\frac{y_i - y_0(x_i)}{\sigma_i}\right]^2 \tag{15}$$

We also define $\chi^2_\nu \equiv \chi^2/(\text{Number of measurements} - \text{Number of parameters estimated})$ where the denominator is the *number of degrees of freedom.* We want P to be large, but even with a large P, χ^2_ν should be close to unity. A large χ^2_ν means either that the fit is poor, *i.e.*, the model doesn't agree with the measurements, or that the errors have been underestimated.

We turn now to the more general case of correlated errors. The χ^2 defined above is only valid if the errors in the variables are independent. Thus, when we have correlated errors, we must re-write χ^2 as follows

$$\chi^2 \equiv (\vec{s} - \vec{t})^T \mathbf{M}^{-1} (\vec{s} - \vec{t}). \tag{16}$$

Here $\mathbf{M}$ is the covariance matrix of the data, $\vec{s}$ the signal and $\vec{t}$ the mathematical incarnation of our model. Often the theoretical model predicts correlation so that the full covariance matrix has the form:

$$\mathbf{M} \equiv [\text{Independent errors}] + [\text{Correlated errors}] + [\text{Theoretical errors}] \tag{17}$$

$$\Leftrightarrow$$

$$M_{qr} \equiv < (s_q - \overline{s}_q)(s_r - \overline{s}_r) > \tag{18}$$

$$\Leftrightarrow$$

$$\begin{aligned} M_{qr} &= \text{cov}(s_q, s_r) \\ M_{qq} &= \sigma_q^2 \end{aligned} \tag{19}$$

3.2 Linear Least Square Fit to a Polynomial

A simple case of regression is a linear fit to a polynomial. We measure x_q and s_q and assume $\sigma_{x,q} \ll \sigma_{s,q}$. Our fitting function is:

$$t_k(\vec{a}) = \sum_{i=1}^{m} a_i \cdot f_i(x_k) \tag{20}$$

where $f_i(x_k)$ could be $(x_k)^{i-1}$ or some more general functions, but are independent of a_i, the parameters we want to fit. Following the method laid out above we go about defining

$$\chi^2 = \sum_{q,r} \left\{ (\vec{t}(\vec{a}) - \vec{s})_q \mathbf{M}^{-1}_{qr} (\vec{t}(\vec{a}) - \vec{s})_r \right\}. \tag{21}$$

To find the minimum of χ^2 we set its derivative to zero.

$$\frac{\partial \chi^2}{\partial a_i} = 2 \sum_{q,r} \left\{ \left(\frac{\partial \vec{t}(\vec{a})}{\partial a_i} \right)_q \mathbf{M}^{-1}_{qr} (\vec{t}(\vec{a}) - \vec{s})_r \right\} = 0 \tag{22}$$

$$\Leftrightarrow$$

$$\sum_{q,r} \left\{ (f_i(x))_q \mathbf{M}^{-1}_{qr} (\vec{t}(\vec{a}) - \vec{s})_r \right\} = 0 \tag{23}$$

$$\Leftrightarrow$$

$$\sum_j a_j \left[\sum_{q,r} \left\{ (f_i(x))_q \mathbf{M}^{-1}_{qr} (f_j(x))_r \right\} \right] = \sum_{q,r} \left\{ (f_i(x))_q \mathbf{M}^{-1}_{qr} (s)_r \right\} \tag{24}$$

To solve equation (24) we let

$$A_{i,j} = \sum_{q,r} \left\{ (f_i(x))_q \mathbf{M}^{-1}_{qr} (f_j(x))_r \right\} \tag{25}$$

and

$$b_i = \sum_{q,r} \left\{ (f_i(x))_q \mathbf{M}^{-1}_{qr} s_r \right\} \tag{26}$$

then

$$\vec{a} = \vec{b}\mathbf{A}^{-1} \tag{27}$$

$$\frac{\partial^2 \chi^2}{\partial a_i \partial a_j} = 2 \sum_{q,r} \left[\left\{ \left(\frac{\partial \vec{t}(\vec{a})}{\partial a_i} \right)_q \mathbf{M}_{qr}^{-1} \left(\frac{\partial \vec{t}(\vec{a})}{\partial a_j} \right)_r \right\} - \left\{ \left(\frac{\partial^2 \vec{t}(\vec{a})}{\partial a_i \partial a_j} \right)_q \mathbf{M}_{qr}^{-1} (\vec{s} - \vec{t}(\vec{a}))_r \right\} \right] \tag{28}$$

$\boldsymbol{\alpha}$ is the curvature matrix:

$$\alpha_{ij} = \frac{1}{2} \frac{\partial^2 \chi^2}{\partial a_i \partial a_j} \tag{29}$$

The error matrix, $\mathbf{C}$, is defined as the inverse of $\boldsymbol{\alpha}$. $\Delta\chi^2_\nu C_{ij}$ are the covariances $<\delta a_i \delta a_j>$ and $\Delta\chi^2_\nu C_{ii}$ are the mean squared errors $(\delta a_i)^2 = \sigma^2_{a_i}$ for the fitted parameters a_i .

$$\mathbf{C} \equiv \boldsymbol{\alpha}^{-1} \tag{30}$$

$$\delta a_i = \sqrt{\Delta\chi^2_\nu} \sqrt{C_{ii}} \tag{31}$$

where $\Delta\chi^2_\nu$ is a change in χ^2 per degree of freedom corresponding to a change in one of the parameters a_i [Press *et al.*].

3.3 The Levenberg-Marquardt Method

The Levenberg-Marquardt method is used to iterate to the optimal χ^2. It combines the Steepest Decent and Grid Search methods into an algorithm with a fast convergence. By Taylor expansion of χ^2 we have

$$\chi^2 = \chi^2(0) + \sum_i \frac{\partial \chi^2}{\partial x_i} x_i + \frac{1}{2} \sum_{i,j} \frac{\partial^2 \chi^2}{\partial x_i \partial x_j} x_i x_j + \dots \tag{32}$$

which we can write as

$$\chi^2 \approx \gamma - \vec{d} \cdot \vec{a} + \frac{1}{2} \vec{a}^T \cdot \mathbf{D} \cdot \vec{a} \tag{33}$$

where $\vec{d}$ is a vector and $\mathbf{D}$ is a square matrix. This leads to

$$a_{\rm min} \approx a_{\rm cur} + \mathbf{D}^{-1} \cdot \left[-\nabla \chi^2(a_{\rm cur}) \right] \tag{34}$$

We measure x_i and s_i. Our fitting function is $\vec{t}(\vec{a})$.

$$\chi^2 = \sum_{q,r} \left\{ (\vec{s} - \vec{t}(\vec{a}))_q \mathbf{M}^{-1}_{qr} (\vec{s} - \vec{t}(\vec{a}))_r \right\} \tag{35}$$

$$\frac{\partial \chi^2}{\partial a_i} = -2 \sum_{q,r} \left\{ \left(\frac{\partial \vec{t}(\vec{a})}{\partial a_i} \right)_q \mathbf{M}^{-1}_{qr} (\vec{s} - \vec{t}(\vec{a}))_r \right\} \tag{36}$$

$$\frac{\partial^2 \chi^2}{\partial a_i \partial a_j} = 2 \sum_{q,r} \left[\left\{ \left(\frac{\partial \vec{t}(\vec{a})}{\partial a_i} \right)_q \mathbf{M}^{-1}_{qr} \left(\frac{\partial \vec{t}(\vec{a})}{\partial a_j} \right)_r \right\} - \left\{ \left(\frac{\partial^2 \vec{t}(\vec{a})}{\partial a_i \partial a_j} \right)_q \mathbf{M}^{-1}_{qr} (\vec{s} - \vec{t}(\vec{a}))_r \right\} \right] \tag{37}$$

Define

$$\beta_i \equiv -\frac{1}{2} \frac{\partial \chi^2}{\partial a_i} \tag{38}$$

and

$$\alpha_{ij} \equiv \frac{1}{2} \frac{\partial^2 \chi^2}{\partial a_i \partial a_j} \tag{39}$$

We approximate α with [Press *et al.*]

$$\alpha_{ij} \approx \sum_{q,r} \left\{ \left(\frac{\partial \vec{t}(\vec{a})}{\partial a_i} \right)_q \mathbf{M}^{-1}_{qr} \left(\frac{\partial \vec{t}(\vec{a})}{\partial a_j} \right)_r \right\} \tag{40}$$

Following equation (33) we have $\boldsymbol{\alpha} = \frac{1}{2}\mathbf{D}$ and we can re-write eq. (34) as

$$\sum_i \alpha_{ij} \delta a_i = \beta_j \tag{41}$$

Let

$$\delta a_i = \frac{1}{\lambda \alpha_{ii}} \beta_i, \tag{42}$$

where λ is a small positive constant and

$$\alpha'_{ii} \equiv \alpha_{ii}(1+\lambda) \tag{43}$$

$$\alpha'_{ij} \equiv \alpha_{ij} \quad (i \neq j) \tag{44}$$

$$\sum_i \alpha'_{ij}\delta a_i = \beta_j, \tag{45}$$

The idea of the Levenberg-Marquardt method is summarized in the following procedure

Step 1: Compute $\chi^2(\vec{a})$.

Step 2: $\lambda \leftarrow 0.001$.

Step 3: Solve the linear equations (45) for $\delta\vec{a}$ and evaluate $\chi^2(\vec{a}+\delta\vec{a})$.

Step 4: If $\chi^2(\vec{a}+\delta\vec{a})$ is smaller than a certain threshold, then stop.

Step 5a: If $\chi^2(\vec{a}+\delta\vec{a}) \geq \chi^2(\vec{a})$, *increase* λ by a factor 10. Go to Step 3.

Step 5b: If $\chi^2(\vec{a}+\delta\vec{a}) < \chi^2(\vec{a})$, *decrease* λ by a factor 10. Go to Step 3.

We also need to calculate the standard deviations, δa_i,

$$\mathbf{C} = \boldsymbol{\alpha}^{-1} \tag{46}$$

and thus,

$$\delta a_i = \sqrt{\Delta\chi^2_\nu}\sqrt{C_{ii}}, \tag{47}$$

where $\Delta\chi^2_\nu$ is a change in χ^2 per degree of freedom corresponding to a change in one of the parameters a_i.

The Levenberg-Marquardt method was applied to the CMB datasets with great success. The method has several times more rapid convergence than the Steepest Descent and Grid Search methods. The latter two were tried first, but neither had reasonable convergence times, as they were implemented.

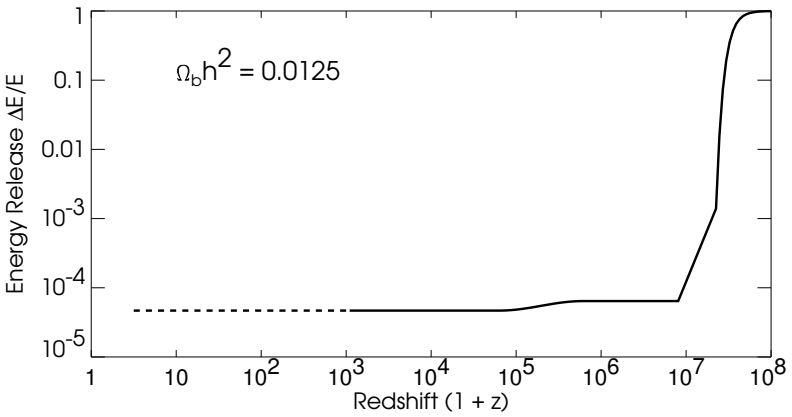

Figure 4: Upper limits (95% CL) on fractional energy ($\Delta E/E_{CBR}$) releases. Ω_b is the baryon number density and h is the hubble constant per 100 km s^{-1} Pc^{-1} .

4 Analysis of the Cosmic Microwave Background Spectrum

A novelty of this analysis has been to use the dependence of frequency for the distortions of the dipole in the fits. This dependency was previously discussed by [Smoot 1980]. Using the dipole data in the fit only marginally improved the fit, however. This is due to the placement of the dipole measurements in frequency space. Figure 3 shows where the current measurements lie and where the distortions are significant. As can be seen in Figure 3, the dipole may play a bigger role in determining the parameters of the distortions when more measurements, with much greater precision or in the region below 10 GHz, become available. Using the dipole does provide an independent check of the spectrum data.

Figure 4 shows upper limits (95% CL) on fractional energy ($\Delta E/E_{CBR}$) releases as set by lack of CMB spectral distortions resulting from processes at different epochs. These can be translated into constraints on the mass, lifetime and photon branching ratio of unstable

relic particles, with some additional dependence on cosmological parameters such as $\Omega_{\rm b}$, the baryon number density [Wright *et al.* 1994, Hu & Silk 1993].

4.1 Lower Limits on the Distortions

Observations show that the universe is ionized [Haiman & Loeb 1997]. This creates Bremsstrahlung and we can set a lower limit on the free-free distortion to $Y_{\rm ff} \sim 2 \times 10^{-6}$. This turns into an added temperature of $\Delta T_{\rm ff} > 0.15$ mK at 2 GHz (as low as one can go in frequency, due to emmisions from the galaxy). This result only takes into account the observed baryons. The real distortion is bigger, because we didn't include Bremsstrahlung that occured at earlier epochs.

A lower limit on the Compton distortion is obtained from measurements of the Sunyaev-Zeldovich effect [Sunyaev & Zeldovich 1970]. The effect creates a y for paths that go through the cores of galactic clusters. Ionized gases in these potential wells Compton-scatter the passing photons. Integrating over the full sky, y is of the order of 10^{-6} [Colafrancesco *et al.* 1997].

Density fluctuations in the early universe oscillate as acoustic waves and are damped by photon diffusion [Silk 1968]. The energy dissipated in this manner is added to the radiation field and gives rise to a non-zero chemical potential. Depending on the nature of the density fluctuations, μ will lie between 2×10^{-8} and a few times 10^{-5} [Hu *et al.* 1994].

4.2 The Data

All published data, from Penzias's & Wilson's first measurement [Penzias & Wilson 1965] of 3K through the recent ground-breaking COBE FIRAS [Fixsen *et al.* 1996] and

DMR [Lineweaver *et al.* 1996] measurements, are used in this analysis. The data used can be found in Tables 5 to 7.

We increased the error estimates of a few of the FIRAS and UBC points at high frequencies to account for possible systematic errors, specifically galactic dust emmision removal. It is these expanded error estimates that are given in Tables 5 and 6.

5 Future Experiments

Since the distortions are frequency dependent an absence of them at millimeter and sub-mm wavelengths does *not* imply correspondingly small distortions at centimeter wavelengths. A better understanding of galactic dust emissions, especially at longer wavelengths, would help produce tighter limits on the disortion parameters. It would be difficult to improve on the COBE measurements without getting above the atmosphere. There are, nevertheless, proposals for new experiments that will measure the CMB.

ARCADE (Absolute Radiometer for Cosmology, Astrophysics, and Diffuse Emission) is a balloon-borne instrument designed to make measurements in the middle of the spectrum. The first flight will have two channels at 10 and 30 GHz. Later incarnations will measure the spectrum at 2, 4, 6, 10, 30 and 90 GHz.

The anticipated measurement sensitivity is 1 mK from a balloon, limited by the ability to estimate/measure emissions from the atmosphere, balloon, flight train, and Earth. ARCADE is thus also a hardware development project for the proposed eventual space mission, DIMES, see below.

The Diffuse Microwave Emission Survey (DIMES) has been selected for a mission concept study for NASA's New Mission Concepts for Astrophysics program [Kogut

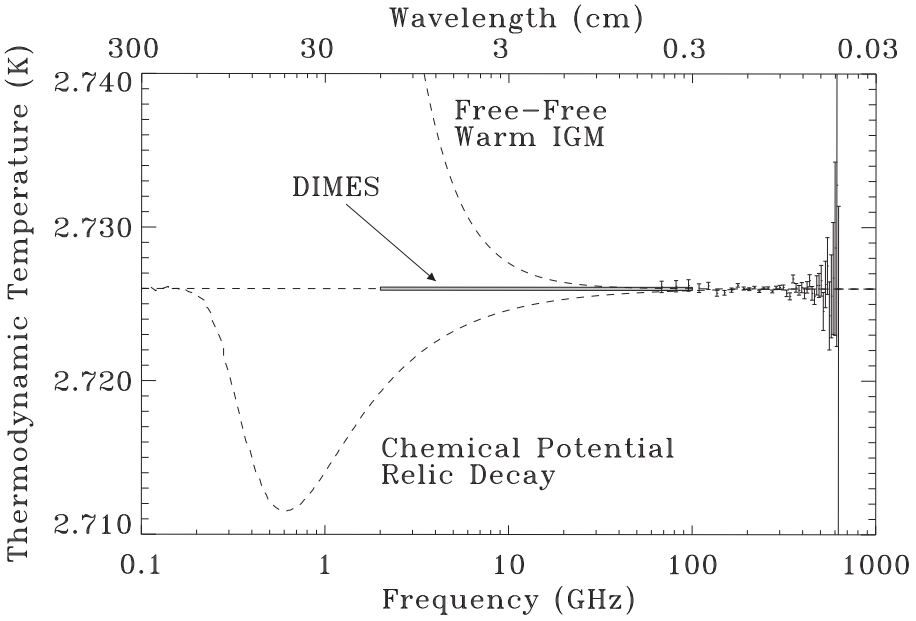

Figure 5: Current 95% confidence upper limits to distorted CMB spectra appear as dashed lines. The FIRAS data and DIMES 0.1 mK error box are also shown; error bars from existing cm-wavelength measurements are larger than the figure height.

1996, http://ceylon.gsfc.nasa.gov/DIMES/index.html]. DIMES will measure the frequency spectrum of the cosmic microwave background and diffuse Galactic foregrounds at centimeter wavelengths to 0.1% precision (0.1 mK). Note that this should detect the free-free distortion, the lower limit of which was mentioned in section 4.1. The FIRAS measurement at sub-mm wavelengths shows no evidence for Compton heating from a hot IGM (Inter-Galactic Medium). Since the Compton parameter $y \propto n_e T_e$, the IGM at high redshift must not be very hot ($T_e \sim 10^5$ K) or reionization must occur relatively recently ($z_{\rm ion} < 10$). DIMES will provide a definitive test of these alternatives. Since the free-free distortion $Y_{\rm ff} \propto n_e^2/\sqrt{T_e}$, lowering the electron temperature *increases* the spectral distortion [Bartlett & Stebbins 1991]. Figure 5 shows the limit to $z_{\rm ion}$ that could be established from the combined DIMES

and FIRAS spectra, as a function of the DIMES sensitivity. A spectral measurement at centimeter wavelengths with 0.1 mK precision can detect the free-free signature from the ionized IGM, allowing direct detection of the onset of hydrogen burning.

6 Summary

None of the distortions, $y, Y_{\rm ff}$ or μ, are larger than the current errors in measurement for the monopole and dipole CMB spectra. The monopole CMB spectrum is very close to a blackbody spectrum. This is strong evidence of the validity of the hot Big Bang model [Smoot 1996], because there are roughly 10^9 photons to each baryon in the universe, and it is very difficult to produce the CMB in astrophysical processes such as the absorption and re-emission of starlight by cold dust, or the absorption or emission by plasmas, and still produce such a precise black body spectrum.

The dipole data did not significantly improve on the errors, but were consistent with and an independent check of the monopole data. Future measurements of the dipole could potentially contribute to tightening the limits or detecting distortions. The PLANCK measurements of the dipole could, in principle, determine the distortions to approximately the same precision as the monopole measurements do now.

7 Acknowledgments

I would like to express my sincere appreciation to my advisor, Dr. George Smoot (LBNL/UC Berkeley), whose enthusiasm and deep knowledge made this work a true pleasure for me. Some of the wordings in sections 1 and 5 have been borrowed from Dr. Smoot's previous works.

I also thank my colleague and friend, Dr. S.Y. Frank Chu (LBNL), for his insight into numerical programming and for teaching me FORTRAN.

A Physics

Concepts are listed in alphabetical order.

Most parameters with a subscript of 0, in cosmology, refer to entities of today, *i.e.*, at redshift $z = 0$. Thus T_0 is the temperature of the Cosmic Microwave Background (CMB). T_0 is sometimes also written as $T_{\rm CMB}$.

The dipole is discribed by

$$\beta \equiv \frac{v}{c}. \tag{48}$$

Black body spectrum (Planck distribution): The distribution of light of a black body follows

$$I(\nu)d\nu = \frac{h\nu^3 d\nu}{\pi^2 c^2 \left(e^{h\nu/kT} - 1\right)}, \tag{49a}$$

where h is Planck's constant, ν is the frequency of the electromagnetic radiation, *i.e.*, of the photons, T is the temperature of the CMB, k is Boltzmann's constant and c is the speed of light in vacuum. A derivation of this formula is found in, *e.g.*, *The Feynman Lectures on Physics* by Feynman, Leighton and Sands on pages 41-3 to 41-7. Black body brightness is the integral over frequency of (49) giving

$$B_\nu \left(x \equiv \frac{h\nu}{kT} \right) = \frac{2h\nu^3}{c^2} \frac{1}{e^x - 1}. \tag{49b}$$

x is called the dimensionless frequency. In the Rayleigh-Jeans region $x \ll 1$, and we can approximate

$$B_\nu(T) = \frac{2h\nu^2}{c^2} kT \qquad\qquad (x \ll 1) \tag{50}$$

The generalization of equation (50) to any ν defines the antenna temperature, $T_{\rm ant}$

$$B_\nu(T_{\rm ant}) = \frac{2h\nu^2}{c^2} kT_{\rm ant}(\nu) \tag{51}$$

The photons in a black body are in *statistical equilibrium*. *Thermodynamic equilibrium* is different from statistical and means that two bodies have the same temperature.

Bremsstrahlung occurs when a charged particle accelerates or decelerates.

Decoupling of some particle means that there is no longer enough energy around to create and destroy that particle.

Distortion parameters (see also section 2.1 The Distortions):
$Y_{\rm ff}$ – a measure of the effects of Bremsstrahlung, unitless; a.k.a. $J_{\rm ff}$
y – a measure of the effects of Compton scattering, unitless
μ_0 – describes the Bose-Einstein distortion, unitless.

Nucleosynthesis is the process of formation of nuclei from protons and neutrons.

$$\textit{Redshift}: \quad z \equiv \frac{\lambda_{\rm obs} - \lambda_{\rm rest}}{\lambda_{\rm rest}} = \frac{\nu_{\rm rest} - \nu_{\rm obs}}{\nu_{\rm obs}} \tag{52}$$

B Statistics

The *standard deviation* of a sample population, s, is defined by

$$s^2 \equiv \frac{1}{N-M} \sum (x_i - \overline{x})^2 \tag{53}$$

where N is the number of measurements and M is the number of parameters to fit. $N - M$ is called the *degrees of freedom* [Press *et al.*].

REFERENCES

Alpher, R.A. and Herman, R.C., Physics Today, 1988, **41**, No. **8**, 24

Astronomical Journal **111**, 794, 1996

Bartlett, J.G., and A. Stebbins, 1991, Astrophysical Journal, **371**, 8

Colafrancesco, C., Mazzotta, P., Rephaeli, Y. and Vittorio, N., 1997, astro-ph/9703121

Danese, L. and De Zotti, G. 1982, *Astr. Ap.*, **107**, 39

Dicke, R.H, Peebles, P.J.E., Roll, P.G. and Wilkinson, D.T., 1965, Astrophysical Journal, **142**, 414

De Amici *et al.* 1991, Astrophysical Journal, **381**, 341

Fixsen, D.J., Cheng, J.M, Mather, J.C., Shafer, R.A. , and Wright, E.L. 1996, Astrophysical Journal **486**, 623, astro-ph/96050504,

Forman, M.A. 1970, Planet. Space Sci. **18**, 25

Gush, H., *et al.* 1990, Phys. Rev. Lett, **65**, 537

Haiman, Z., & Loeb, A., 1997, Astrophysical Journal, **483**, 484

Hu, W., and Silk, J., 1993, Phys. Rev., **170**, 2661

Hu, W., Scott, D. and Silk, J., 1994 Astrophysical Journal, **430**, L5-L8

Kogut *et al.* 1990, Astrophysical Journal **355**, 102

Kogut, A., XVI Moriond CMB Conference Proceedings, astro-ph/9607100 (1996)

Lineweaver, C.H., Tenorio, L, Smoot, G.F, Keegstra, P., Banday, A.J. & Lubin, P. 1996 Astrophysical Journal, **470**, 38-42

Mather *et al.* 1990, Astrophysical Journal Lett, **354**, L37

Peebles, P.J.E., "Principles of Physical Cosmology", Princeton University Press, 1993

Penzias, A.A. and Wilson, R., 1965, Astrophysical Journal, **142**, 419

Press, W.H., *et al.* Numerical Recipes "The Art of Scientific Computing", first ed.

Silk, J., 1968, Astrophysical Journal, **150**, L1

Smoot, G.F. 1980, Physica Scripta, **21**, 619

Smoot, G.F., Levin, S.M., Witebsky, C., De Amici, G. and Rephaeli, Y. 1988, Astrophysical Journal, **331**, 653-659

Smoot, G.F. 1996, Phys. Rev. D vol **54**, 118

Sunyaev, R.A. & Zeldovich, Y.B. 1970, Astroph. Sp. Sci., **7**, 3

Sunyaev, R.A. & Zeldovich, Y.B. 1980, Ann. Rev. of Astron. & Astroph. **18**, 537

Wright, E.L., *et al.*, 1994, Astrophysical Journal, **420**, 450

This manuscript was prepared with the AAS WGAS LaTeX macros v1.0

Dipole References

Bennett, C.L., et al. 1994, Astrophysical Journal, **436**, 423

Bennett, C.L., et al. 1996, Astrophysical Journal, **464**, L1-4

Boughn, S.P. et al. 1971, Astrophysical Journal, **165**, 439

Boughn, S.P. et al. 1981, Astrophysical Journal, **243**, L113

Cheng, E.S. et al. 1979, Astrophysical Journal, **232**, L139

Cheng, E.S. 1983 Ph.D. thesis, Princeton Univ.

Conklin, E.K. 1969, Nature, **222**, 971

Conklin, E.K. 1972, IAU Symposium 44, ed. D.S. Evans (Dordrecht: Reidel), 518

Corey, B.E. 1978, Ph.D. thesis Princeton U.

Corey, B.E. & Wilkinson D. T., 1976, Bull. Amer. Astron. Soc, **8**, 351

Cottingham, D.A. 1987, Ph.D. thesis, Princeton Univ.

Fabbri, R., et al. 1980, Phys. Rev. Let., 44, 1563, erratum 1980, Phys. Rev. Let., **45**, 401

Fixsen, D.J., Cheng, E.S. & Wilkinson, D.T. 1983, Phys. Rev. Let., **50**, 620

Fixsen, D.J., et al. 1994, Astrophysical Journal, **420**, 445

Fixsen, D.J., et al. 1996, Astrophysical Journal, **486**, 623

Ganga, K., Cheng, E., Meyer, S., Page, L. 1993, Astrophysical Journal, **410**, L57

Gorenstein, M.V. 1978, Ph.D. thesis, U.C. Berkeley

Halpern, M., et al. 1988 Astrophysical Journal, **332**, 596

Henry, P.S. 1971, Nature, **231**, 516

Kogut, A., et al. 1993, Astrophysical Journal, **419**, 1

Lineweaver, C.H., et al. 1995, Astrophysical Letters and Comm., **32**, 173-181

Lineweaver, C.H., et al. 1996, Astrophysical Journal, **470**, 38

Lubin, P.M., Epstein, G.L., Smoot, G.F. 1983, Phys. Rev. Let., **50**, 616

Lubin, P.M. et al. 1985, Astrophysical Journal, **298**, L1

Meyer, S.S., et al. 1991, Astrophysical Journal, **371**, L7

Muehler, D. 1976, in Infrared and Submillimeter Ast., ed G.Fazio, D.Reidel, Dordrecht, 63

Partridge, R.B. & Wilkinson, D. T., 1967, Phys. Rev. Let.**18**, 557

Penzias, A.A. & Wilson, R. W. 1965, Astrophysical Journal, **142**, 419

Smoot, G.F., Gorenstein, M. V. & Muller, R. A. 1977, Phys. Rev. Let., **39**, 898

Smoot, G.F. & Lubin, P. 1979, Astrophysical Journal, **234**, L83

Smoot, G.F., et al. 1991, Astrophysical Journal, **371**, L1

Smoot, G.F., et al. 1992, Astrophysical Journal, **396**, L1

Strukov, I.A., Skulachev, D.P. 1984, Sov. Ast. Lett. **10**, 3

Strukov, I.A., Skulachev, D.P., Boyarskii, M.N., Tkachev, A.N. 1987, Sov. Ast. Lett. **13**, 2

Wilkinson, D.T. & Partridge, R.B. 1969, Partridge quoted in American Scientist, **57**, 37

Table 3: All dipole data used in the fits. Coordinates are galactic.

	Amplitude		Longitude		Latitude		Freq
	[mK]	+-sigma	l [deg]	+-sigma	b [deg]	+-sigma	[GHz]
Penzias & Wilson (1965)	<270						4
Partridge & Wilkinson (1967)	0.8	2.2					9
Wilkinson & Partridge (1969)	1.1	1.6					9
Conklin (1969)	1.6	0.8	96	30	85	30	8
Boughn *et al.* (1971)	7.6	11.6					37
Henry (1971)	3.3	0.7	270	30	24	25	10
Conklin (1972)	>2.28	0.92	195	30	66	10	8
Corey & Wilkinson (1976)	2.4	0.6	306	28	38	20	19
Muehler (1976)	2.0	1.8	207		-11		150
Smoot *et al.* (1977)	3.5	0.6	248	15	56	10	33
Corey (1978)	3.0	0.7	288	26	43	19	19
Gorenstein (1978)	3.60	0.5	229	11	67	8	33
Cheng *et al.* (1979)	2.99	0.34	287	9	61	6	30
Smoot & Lubin (1979)	3.1	0.4	250.6	9	63.2	6	33
Fabbri *et al.* (1980)	2.9	0.95	256.7	13.8	57.4	7.7	300
Boughn *et al.* (1981)	3.78	0.30	275.4	3.9	46.8	4.5	46
Cheng (1983)	3.8	0.3					30
Fixsen *et al.* (1983)	3.18	0.17	265.7	3.0	47.3	1.5	25
Lubin (1983)	3.4	0.2					90
Strukov *et al.* (1984)	2.4	0.5					67
Lubin *et al.* (1985)	3.44	0.17	264.3	1.9	49.2	1.3	90
Cottingham (1987)	3.52	0.08	272.2	2.3	49.9	1.5	19
Strukov *et al.* (1987)	3.16	0.07	266.4	2.3	48.5	1.6	67
Halpern *et al.* (1988)	3.4	0.42	289.5	4.1	38.4	4.8	150
Meyer *et al.* (1991)			249.9	4.5	47.7	3.0	170
Smoot *et al.* (1991)	3.3	0.1	265	1	48	1	53
Smoot *et al.* (1992)	3.36	0.1	264.7	0.8	48.2	0.5	53
Ganga *et al.* (1993)			267.0	1.0	49.0	0.7	170
Kogut *et al.* (1993)	3.365	0.027	264.4	0.3	48.4	0.5	53
Fixsen *et al.* (1994)	3.347	0.008	265.6	0.75	48.3	0.5	300
Bennett *et al.* (1994)	3.363	0.024	264.4	0.2	48.1	0.4	53
Bennett *et al.* (1996)	3.353	0.024	264.26	0.33	48.22	0.13	53
Fixsen *et al.* (1996)	3.372	0.005	264.14	0.17	48.26	0.16	300
Lineweaver *et al.* (1996)	3.358	0.023	264.31	0.17	48.05	0.10	53

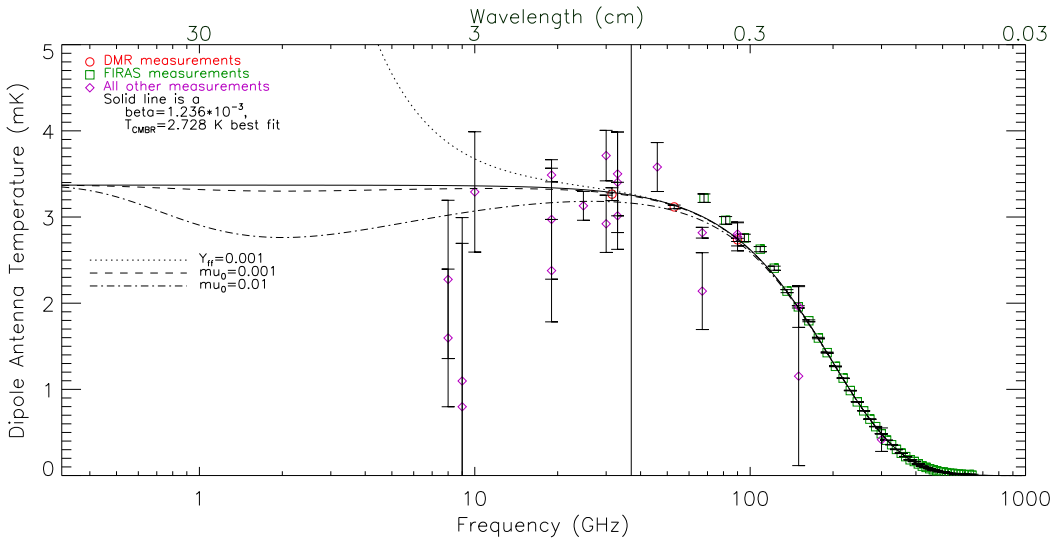

Figure 6: Antenna temperature as a function of frequency for the CMB dipole with distortions.

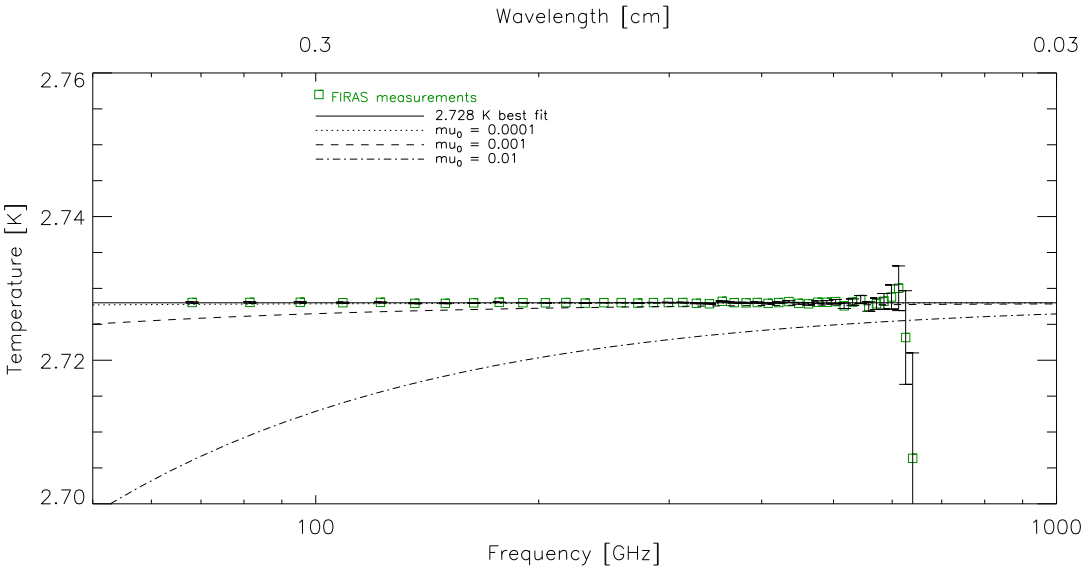

Figure 7: Thermodynamic temperature as a function of frequency of the CMB monopole. This is a close-up of Fig. 2 showing the FIRAS measurements.

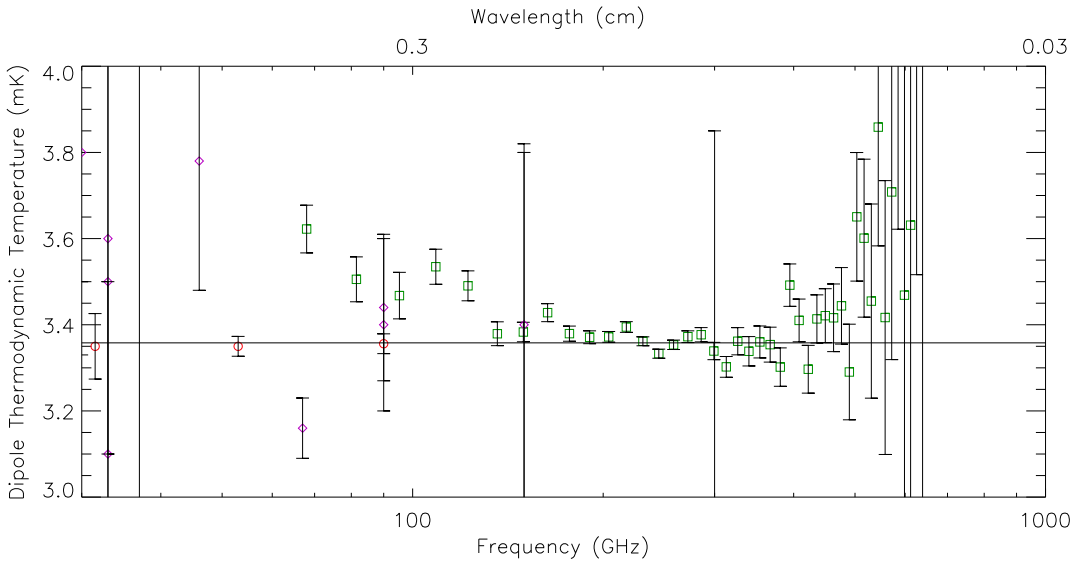

Figure 8: Thermodynamic temperature as a function of frequency of the CMB dipole. This is a close-up of Fig. 3. Note the position and small errors of the COBE/DMR measurements (circles) compared to COBE/FIRAS (squares) and other measurements (diamonds).

Table 4: Measurements of $T_{\rm CMB}$ for the monopole

Frequency (GHz)	Wavelength (cm)	Temperature (K)	Type	Reference
0.408	73.5	3.7 ± 1.2	Ground (LN)	Howell & Shakeshaft 1967, Nature, 216, 753.
0.6	50	3.0 ± 1.2	Ground (Term)	Sironi et al. 1990, Ap.J., 357, 301.
0.610	49.1	3.7 ± 1.2	Ground (LN)	Howell & Shakeshaft 1967, Nature, 216, 7
0.635	47.2	3.0 ± 0.5	Ground (LN)	Stankevich et al 1970, Australian J. Phys, 23, 529
0.820	36.6	2.7 ± 1.6	Ground (Term)	Sironi et al. 1991, Ap.J., 378, 550.
1	30	2.5 ± 0.3	Ground (LN)	Pelyushenko & Stankevich 1969, Sov. Astron., 13, 223.
1.4	21.3	2.11 ± 0.38	Ground (CLC)	Levin et al. 1988, Ap.J., 334,14
1.42	21.2	3.2 ± 1.0	Ground (Term)	Penzias and Wilson 1967, AJ, 72, 315
1.43	21	$2.65^{+0.33}_{-0.30}$	Ground (LN)	Staggs et al. 1996, ApJ, 458, 407
1.44	20.9	2.5 ± 0.3	Ground (LN)	Pelyushenko & Stankevich 1969, Sov. Astron., 13, 223.
1.45	20.7	2.8 ± 0.6	Ground (Term)	Howell & Shakeshaft 1966, Nature, 210, 1318.
1.47	20.4	2.27 ± 0.19	Ground (CLC)	Bensadoun et al. 1993, Ann. NY Acad. Sci, 668, p792-4
2	15	2.5 ± 0.3	Ground (LN)	Pelyushenko & Stankevich 1969, Sov. Astron., 13, 223.
2	15	2.55 ± 0.14	Ground (CLC)	Bersanelli *et al.*, 1994, Ap.J., 424, 517
2.3	13.1	2.66 ± 0.77	Ground (Term)	Otoshi & Stelzreid 1975, IEEE Trans on Inst & Meas, 24, 174.
2.5	12	2.71 ± 0.21	Ground (CLC)	Sironi et al. 1991, Ap. J., 378, 550.
3.8	7.9	2.64 ± 0.06	Ground (CLC)	De Amici et al. 1991, Ap.J., 381, 341.
4.08	7.35	3.5 ± 1.0	Ground (Term)	Penzias & Wilson 1965, Ap.J., 142, 419.
4.75	6.3	2.70 ± 0.07	Ground (CLC)	Mandolesi et al. 1986, Ap.J., 310, 561.
7.5	4.0	2.60 ± 0.07	Ground (CLC)	Kogut et al. 1988, Ap.J., 355, 102
7.5	4.0	2.64 ± 0.06	Ground (CLC)	Levin et al. 1992, Ap.J., 396, 3
9.4	3.2	3.0 ± 0.5	Ground (Term)	Roll & Wilkinson 1966, Phys. Rev. Lett., 16, 405.
9.4	3.2	$2.69^{+0.16}_{-0.21}$	Ground (CLC)	Stokes et al. 1967, Phys. Rev. Lett., 19, 1199.
10	3.0	2.62 ± 0.06	Ground (CLC)	Kogut et al. 1990, Ap.J., 355, 102.
10.7	2.8	2.730 ± 0.014	Balloon (LHe)	Staggs et al. 1996, Ap.J., 473, L1
19.0	1.58	$2.78^{+0.12}_{-0.17}$	Ground (CLC)	Stokes et al. 1967, Phys. Rev. Lett., 19, 1199.
20	1.5	3.0 ± 0.4	Ground (CLC)	Welch et al. 1967, Phys. Rev. Lett. 18, 1068

Table 4: Measurements of $T_{\rm CMB}$ for the monopole *continued*

Frequency (GHz)	Wavelength (cm)	Temperature (K)	Type	Reference
31.5	0.95	2.83 ± 0.07	COBE/DMR	Kogut et al. 1996, Ap.J, 470, 653
32.5	0.924	3.16 ± 0.26	Ground (CLC)	Ewing et al. 1967, Phys. Rev. Lett, 19, 1251.
33.0	0.909	2.81 ± 0.12	Ground (CLC)	De Amici et al. 1985, Ap.J., 298, 710.
35.0	0.856	$2.56^{+0.17}_{-0.22}$	Ground (CLC)	Wilkinson 1967, Phys. Rev. Lett., 19, 1195.
37	0.82	2.9 ± 0.7	Ground (LN)	Puzanov et al. 1968, Sov. Astr., 11, 905.
53	0.57	2.71 ± 0.03	COBE/DMR	Kogut et al. 1996, Ap.J, 470, 653
83.8	0.358	2.4 ± 0.7	Ground (LN)	Kislyakov et al. 1971, Sov. Ast., 15, 29.
90	0.33	$2.46^{+0.40}_{-0.44}$	Ground (CLC)	Boynton et al. 1968, Phys. Rev. Lett., 21, 462.
90	0.33	2.61 ± 0.25	Ground (CLC)	Millea et al. 1971, Phys. Rev. Lett., 26, 919.
90	0.33	2.48 ± 0.54	Plane (Term)	Boynton & Stokes 1974, Nature, 247, 528.
90	0.33	2.60 ± 0.09	Ground (CLC)	Bersanelli et al. 1989, Ap.J., 339, 632.
90	0.33	2.712 ± 0.020	Ground (CLC)	Schuster et al. UC Berkeley PhD Thesis
90	0.33	2.72 ± 0.04	COBE/DMR	Kogut et al. 1996, Ap.J, 470, 653
90.3	0.332	< 2.97	Balloon	Bernstein et al. 1990, Ap.J., 362, 107.
113.6	0.264	2.70 ± 0.04	CN (z Per)	Meyer & Jura 1985, Ap.J., 297, 119.
113.6	0.264	2.74 ± 0.05	CN (z Oph)	Crane et al. 1986, Ap.J., 309, 12.
113.6	0.264	2.76 ± 0.07	CN (HD 21483)	Meyer et al. 1989, Ap.J. Lett, 343, L1.
113.6	0.264	$2.796^{+0.014}_{-0.039}$	CN (z Oph)	Crane et al. 1989, Ap.J., 346, 136.
113.6	0.264	2.75 ± 0.04	CN (z Per)	Kaiser & Wright 1990, Ap.J. Lett, 356, L1.
113.6	0.264	2.834 ± 0.085	CN (HD 154368)	Palazzi et al. 1990, Ap.J., 357, 14.
113.6	0.264	2.807 ± 0.025	CN (16 stars)	Palazzi et al. 1992, Ap.J., 398, 53.
113.6	0.264	$2.279^{+0.023}_{-0.031}$	CN (5 stars)	Roth et al. 1993, Ap.J., 413, L67.
154.8	0.194	< 3.02	Balloon	Bernstein et al. 1990, Ap.J., 362, 107.
195.0	0.154	< 2.91	Balloon	Bernstein et al. 1990, Ap.J., 362, 107.
227.3	0.132	2.656 ± 0.057	CN (5 stars)	Roth et al. 1993, Ap.J., 413, L67.
227.3	0.132	2.76 ± 0.20	CN (z Per)	Meyer & Jura 1985, Ap.J., 297, 119.
227.3	0.132	$2.75^{+0.24}$	CN (z Oph)	Crane et al. 1986, Ap.J., 309, 822.

Table 5: FIRAS Data; Fixsen *et al.* 1996

Frequency GHz	Temperature K	Upper Error K	Lower Error K
68.1	2.72804	.00011	.00011
81.5	2.72805	.00011	.00011
95.3	2.72807	.00011	.00011
108.8	2.72801	.00009	.00009
122.3	2.72806	.00007	.00007
136.1	2.72792	.00006	.00006
149.6	2.72792	.00005	.00005
163.4	2.72798	.00004	.00004
176.9	2.72807	.00004	.00004
190.4	2.72801	.00003	.00003
204.2	2.72800	.00003	.00003
217.6	2.72803	.00002	.00002
231.1	2.72795	.00002	.00002
244.9	2.72802	.00002	.00002
258.4	2.72802	.00002	.00002
272.2	2.72795	.00003	.00003
285.7	2.72802	.00003	.00003
299.2	2.72803	.00004	.00004
313.0	2.72803	.00005	.00005
326.5	2.72792	.00006	.00006
340.0	2.72786	.00007	.00007
353.8	2.72820	.00008	.00008
367.2	2.72802	.00008	.00008

Table 5: FIRAS Data; Fixsen *et al.* 1996 – *continued*

Frequency GHz	Temperature K	Upper Error K	Lower Error K
381.0	2.72798	.00009	.00009
394.5	2.72803	.00010	.00010
408.0	2.72792	.00010	.00010
421.8	2.72803	.00011	.00011
435.3	2.72816	.00012	.00012
448.8	2.72792	.00013	.00013
462.6	2.72785	.00015	.00015
476.1	2.72807	.00019	.00019
489.9	2.72807	.00023	.00023
503.4	2.72816	.00030	.00030
516.8	2.72757	.00037	.00037
530.6	2.72809	.00045	.00045
544.1	2.72845	.00055	.00055
557.9	2.72748	.00066	.00066
571.4	2.72786	.00080	.00080
584.9	2.72821	.00108	.00108
598.7	2.72880	.00168	.00168
612.2	2.73002	.00311	.00311
625.7	2.72316	.00652	.00652
639.5	2.70634	.01468	.01468

Table 6: UBC COBRA Rocket Data; Gush *et al.* 1990

Frequency GHz	Temperature K	Upper Error K	Lower Error K
54.6	2.789	.100	.100
68.1	2.648	.100	.100
81.8	2.664	.100	.100
95.3	2.737	.010	.010
109.1	2.718	.010	.010
122.6	2.724	.010	.010
136.4	2.753	.010	.010
149.9	2.736	.010	.010
163.7	2.724	.010	.010
177.2	2.735	.010	.010
191.0	2.731	.010	.010
204.5	2.725	.010	.010
218.2	2.734	.010	.010
231.7	2.737	.010	.010
245.5	2.735	.010	.010
259.0	2.733	.010	.010
272.8	2.733	.010	.010
286.3	2.735	.010	.010
300.1	2.735	.010	.010
313.6	2.742	.010	.010
327.4	2.754	.010	.010
340.9	2.743	.010	.010

Table 6: UBC COBRA Rocket Data; Gush *et al.* 1990 – *continued*

Frequency GHz	Temperature K	Upper Error K	Lower Error K
354.7	2.734	.010	.010
368.1	2.751	.010	.010
381.9	2.752	.010	.010
395.4	2.739	.010	.010
409.2	2.752	.010	.010
422.7	2.772	.010	.010
436.5	2.747	.010	.010
450.0	2.755	.010	.010
463.8	2.762	.010	.010
477.3	2.686	.100	.100
491.1	2.637	.100	.100
504.6	2.683	.100	.100
518.3	2.732	.100	.100
531.8	2.713	.100	.100
545.6	2.719	.100	.100
559.1	2.743	.100	.100
572.9	2.717	.100	.100
586.4	2.723	.100	.100

Table 7: All CMB measurements except FIRAS and UBC COBRA

Frequency GHz	Temperature K	Upper Error K	Lower Error K
.408	3.700	1.200	1.200
.600	3.000	1.200	1.200
.610	3.700	1.200	1.200
.635	3.000	.500	.500
.820	2.700	1.600	1.600
1.000	2.500	.300	.300
1.400	2.110	.380	.380
1.420	3.200	1.000	1.000
1.430	2.650	.330	.300
1.440	2.500	.300	.300
1.450	2.800	.600	.600
1.470	2.266	.190	.190
2.000	2.500	.300	.300
2.000	2.550	.140	.140
2.300	2.660	.770	.770
2.500	2.710	.210	.210
3.800	2.640	.060	.060
4.080	3.500	1.000	1.000
4.750	2.700	.070	.070
7.500	2.640	.060	.060
9.400	3.000	.500	.500
9.400	2.690	.160	.210
10.000	2.620	.060	.060
10.700	2.730	.014	.014
19.000	2.780	.120	.170
20.000	2.000	.400	.400

Table 7: All CMB measurements except FIRAS and UBC COBRA – *continued*

Frequency GHz	Temperature K	Upper Error K	Lower Error K
32.500	3.160	.260	.260
33.000	2.810	.120	.120
35.000	2.560	.170	.220
37.000	2.900	.700	.700
53.000	2.710	.030	.030
83.800	2.400	.700	.700
90.000	2.460	.400	.440
90.000	2.610	.250	.250
90.000	2.480	.540	.540
90.000	2.600	.090	.090
90.000	2.712	.020	.020
90.000	2.720	.040	.040
90.300	< 2.97		
113.600	2.700	.040	.040
113.600	2.740	.050	.050
113.600	2.760	.070	.070
113.600	2.796	.014	.039
113.600	2.750	.040	.040
113.600	2.834	.085	.085
113.600	2.807	.025	.025
113.600	2.729	.023	.031
227.300	2.760	.200	.200
227.300	2.750	.240	.290
227.300	2.830	.090	.090
227.300	2.832	.072	.072
227.300	2.656	.057	.057